International Communications in Heat and Mass Transfer 158 (2024) 107905

Contents lists available at ScienceDirect

International Communications in Heat and Mass Transfer

journal homepage: www.elsevier.com/locate/ichmt

A new validated model of dropwise condensation of vapor in humid air flow

Matteo Mirafiori, Marco Tancon *, Stefano Bortolin, Davide Del Col

Dipartimento di Ingegneria Industriale, Università degli Studi di Padova, Via Venezia 1, 35131 Padova, Italy

ARTICLE INFO

Keywords:
Dropwise condensation
Humid air
Numerical simulation
Droplet population
Accommodation coefficient

ABSTRACT

Vapor condensation from humid air can occur as dropwise condensation (DWC). Accurate modeling of DWC is crucial not only to predict heat transfer, but also to understand the underlying mechanisms. The increasing availability of computing resources has led to development of sophisticated numerical models to determine drop-size distribution and heat exchanged, eliminating the need for statistical assumptions. This paper introduces a novel individual-based model (IBM) to perform simulations of DWC with non-condensable gases (NCG). In the developed IBM, the droplet growth rate model and the accommodation coefficient are critical input parameters. Here, we use droplet growth rate measurements (which are rare in the literature) to infer the value of accommodation coefficient and select the best growth rate model for predicting DWC with humid air. Then, the developed simulation tool is successfully validated (within 6%) against an experimental database obtained by varying air humidity (relative humidity 50–90%, specific humidity 0.012–0.022 kg_v/kg_{dryair}) and dew-to-wall temperature difference (7–13 K). After validation, the model is used to study the effect of main input parameters on droplet population and condensation heat flux. Interestingly, the small droplet population is not affected by the accommodation coefficient or air conditions, but instead depends on surface wettability.

1. Introduction

Water vapor condensation from humid air is a ubiquitous two-phase phenomenon involved in several industrial applications [1,2]. Therefore, the enhancement of the heat transfer performance is undoubtedly attractive for both the scientific community and industry. The replacement of traditional filmwise condensation (FWC) with dropwise condensation (DWC) has been identified as a promising solution to enhance the heat transfer during pure steam condensation [3,4]: the heat transfer coefficient (HTC) can be 5–10 times higher compared to FWC [5–7]. On the other hand, in many practical applications, such as the dehumidification of air for thermal comfort in buildings and the harvesting of water from the air, the condensation process involves water vapor in humid air at ambient conditions. The HTC during both DWC and FWC from humid air is severely penalized by the large amount of non-condensable gases (NCGs) accumulated near the liquid-vapor interface, which add a resistance to the diffusion of vapor molecules towards the surface. Although vapor diffusion is the dominant mechanism and, therefore, conduction through the condensate no longer represents the highest thermal resistance (as for pure steam condensation), promoting DWC in presence of humid air may lead to higher HTC compared to FWC [8–10].

Regardless of the presence or absence of NCG, methods for predicting heat flux during DWC usually combine the drop-size distribution on the condensing surface with the heat flux exchanged by each droplet [11–13]. Two different approaches are usually used to obtain the drop-size distribution: solving the population balance theory or performing numerical simulations.

Among the various methods developed to analytically evaluate the average droplet population, the equation by Le Fevre and Rose [14] is usually used to obtain the population of large drops, while the population balance theory (which was first developed by Tanaka [15]) remains the preferred choice to solve the small droplet population. By coupling the average drop-size distribution given by the population balance theory with an equation for the heat flow rate through an individual droplet, the total heat flux exchanged during DWC can be predicted analytically [16]. Hereafter, models based on this approach for the determination of the droplet distribution will be named population-based models (PBM). Even in the case of DWC with humid air, the computational approach based on the population balance theory

* Corresponding author.
E-mail address: marco.tancon@unipd.it (M. Tancon).

https://doi.org/10.1016/j.icheatmasstransfer.2024.107905

Available online 14 August 2024

remains almost the same. However, the expression for the heat transferred by a droplet must take into account the thermal resistance due to vapor diffusion through non-condensable gases [17–19].

The second approach involves running numerical simulations of the droplet lifecycle [20–22]. As each droplet is followed during its growth, from nucleation to disappearance by coalescence or sweeping, the instantaneous drop-size distribution over the computational domain can be evaluated. This methodology is commonly called individual-based modeling (IBM). As shown in prior works [22–24], the average drop-size distribution given by IBM is in good agreement with experimental data for droplet radii from few microns to millimetres. It is important to note that the two approaches yield quite different drop-size distribution, especially in the region of the smaller drops. Unfortunately, due to the limitations of optical methods, there are no reference data for the small droplet population and, therefore, the distribution of small droplets predicted by both IBMs and PBMs has not yet been validated. Because of the mismatch in the predicted drop-size distribution, the heat flux estimated by the two approaches can be quite different, with variations of up to 40% [8,22].

Modeling of DWC from humid air results to be more complex than modeling DWC of saturated steam for three main reasons. Firstly, the diffusion resistance is difficult to mathematically describe, as it strongly depends on the accommodation coefficient α. This parameter defines the fraction of vapor molecules absorbed by the liquid phase out of the total number of molecules impacting the surface. A value of $\alpha = 1$ denotes complete condensation, whereas $\alpha < 1$ represents an incomplete condensation. The lower the accommodation coefficient, the smaller the amount of vapor molecules that condense, and thus the lower the latent heat flux through the surface. In contrast to steam condensation, where the accommodation coefficient is typically assumed to be near unity [17,25], condensation from humid air exhibits lower values of α. According to Marek and Straub [26] and Gleason et al. [27], the accommodation coefficient can vary from 10^{-5} to 1, depending on the environmental conditions. The difficulty of directly measuring the accommodation coefficient contributes to the broad range of values found in the literature. The presence of this additional resistance increases the complexity of single droplet heat transfer models compared to those for steam DWC. Consequently, analytical solutions for the distribution of small drops are intrinsically difficult to obtain and, thus, the contribution of small drops to the overall heat flux is often neglected by analytical models, as in the case of Zheng et al. [17,25]. Secondly, the simplification of single droplet growth, which does not account for the interaction effect between droplets, may result in an overestimation of the condensation rate for diffusion-controlled DWC in the presence of NCG [28,29]. In fact, the growth of small drops close to larger drops is expected to occur at a slower rate due to the local reduction of the condensing vapor. In the literature, few methods have been proposed to take into account this effect for purely diffusive vapor mass transfer (and thus in quiescent humid air) [30,31]. Thirdly, measurements of condensation heat flux during DWC in presence of humid air, which are necessary to validate the models, are rare in the literature. Moreover, as shown by Tancon et al. [8], the few available data are affected by large uncertainties, making any reliable validation very challenging.

In the literature, so far, four IBMs coupled with their own model for the heat flux exchanged by an individual droplet during the DWC of humid air have been presented [17–19,32]. However, it should be noted that each model has significant limitations. These limitations include simulation of a limited number of drops ($\sim 10^5$ drops), absence of drop-size distribution representation, inadequate comparison with experimental data, insufficient analysis of numerical parameters, and significant variability in absolute values between different models. Therefore, it is necessary to validate and compare the different models by varying the operating conditions of humid air, the accommodation coefficient and the nucleation sites density as well as the numerical parameters. The present model addresses these limitations by providing a comprehensive and meticulous validation, serving as a solid foundation for further development and application.

Therefore, this work aims to mark a milestone in the exploration of DWC with humid air, employing both experimental and numerical approaches. The main goal is to provide a reliable computational method to predict the DWC heat flux during air dehumidification. We present a numerical model consisting of a homemade IBM developed in MATLAB and C codes for optimized computational efficiency. The only input parameter of the model to be assumed remains the accommodation coefficient. However, measurements of this parameter are rare and, furthermore, many values are available in the literature because of its dependency on environmental conditions [26,27,33]. By measuring the droplet growth rate under different operating conditions from videos recorded during condensation, we are able to estimate the accommodation coefficient. The developed IBM, coupled with the present estimated values of accommodation coefficient and measurements of nucleation sites density obtained in our previous work [8], is used to simulate DWC of vapor in humid air. Numerical results are compared against both latent heat flux data and videos acquired during DWC at a fixed air temperature (28 °C), while varying relative humidity (50–90%) and dew-to-wall temperature difference (7–13 K). These are typical operating conditions of HVAC dehumidification systems for thermal comfort in buildings. The present experimental data of latent heat flux and drop-size distribution are taken from a previous publication [8]. Instead, the optical measurements used to determine the droplet growth rate represent new data not previously published. After validation, the numerical model is used to get insight into the small droplet distribution, with a focus on its dependency from the main input parameters (accommodation coefficient, thermodynamic conditions, and surface wettability).

2. New model for simulation of DWC in the presence of humid air

The individual-based model (IBM) developed to simulate DWC with humid air is described in detail in this section. In particular, the mathematical modeling of droplet nucleation, growth, coalesce and sliding are described. At the end of the section, the effect of numerical input parameters on numerical results will be investigated.

2.1. Droplet nucleation

At the beginning of the numerical procedure, the nucleation sites are randomly distributed by the IBM within the computational domain and their position is maintained constant for the whole simulation. As depicted in Fig. 1, a random distribution of nucleation sites (Fig. 1a) appears to better approximate the observed distribution (Fig. 1c) compared to a regular distribution (Fig. 1b). Several authors [34,35] have reported that the drop-size density obtained numerically is independent of the initial arrangement of the nucleation sites. However, as reported in the Supplementary Material S1, we found that the distribution of drop-size undergoes slight variations in the range of droplet radii 5–20 μm for a regular distribution of nucleation sites (Fig. 1b).

At each time step, a droplet of radius corresponding to the minimum radius r_{min} is positioned instantly on any available nucleation site. Unless otherwise indicated, r_{min} is evaluated as [36]:

$$r_{min} = \frac{2\,\sigma\,T_{dew}}{\rho_l\,h_{lv}\,(T_{dew} - T_{wall})} \tag{1}$$

where h_{lv} is the latent heat of vaporization, σ the liquid surface tension, T_{dew} the dew temperature, ρ_l the density of liquid phase, and T_{wall} the wall temperature. Although the process of nucleation does not physically occur simultaneously [37], several studies in the literature [38–40] have estimated via molecular dynamics simulations that the time required for nucleation is around 50 ns. During dehumidification, the droplet growth rate and, thus, the heat transfer are severely constrained

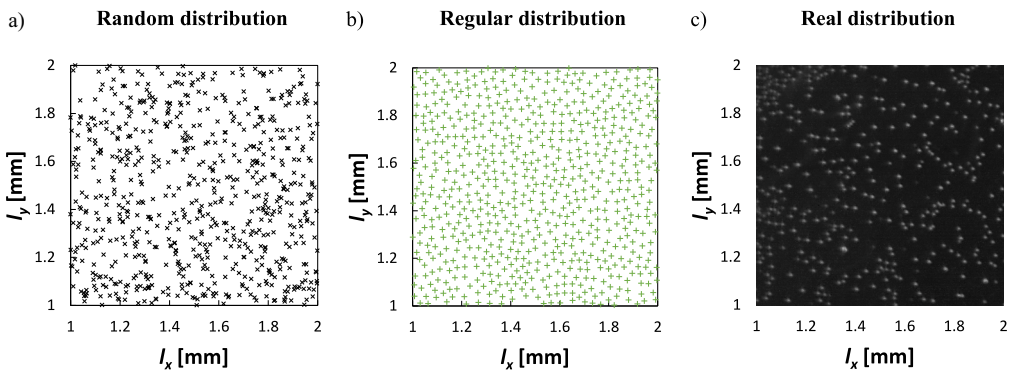

Fig. 1. Example of a) random and b) regular distribution of nucleation sites over the computational domain compared with c) an image taken from Tancon et al. [8] showing the actual distribution of nucleation sites in the early stages of condensation. The computation domain area and the visualized area are 1 × 1 mm^2.

by the diffusion of water vapor through the NCGs layer, resulting in a considerable increase in the time required to complete a condensation cycle (from nucleation to sliding), from about 1 s (pure steam) to 1 h (humid air). This reflects on the choice of the simulation time step. In order to accurately simulate the droplet growth rate from r_{min} to r_{max}, while maintaining a feasible computational time, it is necessary to adopt a time step between 0.001 s and 0.01 s. This aspect will be further discussed in Section 2.5. Since these values of time step (10^{-3} s or 10^{-2} s) are considerably larger than the nucleation time (50 ns), it is reasonable to assume that all available nucleation sites are occupied within a single time step by a droplet with a radius equal to r_{min} (Eq. 1). Thus, the nucleation phase is approximated to be instantaneous.

2.2. Droplet growth

In each time step, the model predicts droplet growth by direct condensation in accordance with a certain model for the heat transferred by an individual droplet. In this work, four models have been considered: Zheng et al. [17], Suzzi and Croce [32], Baghel et al. [18], and Lyu et al. [19]. Specifically, the Zheng et al. [17] model is considered here in its original formulation based on the assumption of single droplet growth. The subsequent modification (described in Zheng et al. [30]) to account for the interaction effect between neighboring droplets has not been included for the sake of simplicity, also considering that the present dataset was not collected during purely diffusion-controlled DWC (see Section 3.1). Among these models, Zheng et al. [17] has been identified as the most reliable option for predicting the present measurements of droplet growth rate during DWC from humid air (see Section 4.1) and the experimental data (both condensation heat flux and drop-size distribution) taken from Tancon et al. [8] (see Section 4.2). Detailed descriptions of the models considered in this work are given in Supplementary Material S2. Once the radius increase of each droplet is determined, the software updates the dimension of the drops. To speed up the calculation, the algorithms have been written in C code and compiled using the MATLAB® mex compiler [41].

Considering the heat transfer model by Zheng et al. [17] and assuming that heat transfer during condensation occurs only through the droplets, the heat flux through a single droplet (q_d) can be equated with the mass flux of the condensing vapor to evaluate the droplet growth rate ($G = \mathrm{d}r/\mathrm{d}t$):

$$q_d = \rho_l h_{lv} \left(2 - 3cos\theta + cos^3\theta\right) G \tag{2}$$

where θ is the droplet static contact angle. All the thermodynamic properties are obtained by means of REFPROP v10 [42].

After updating the dimensions of all the droplets, some of them may overlap. This triggers the second phenomenon of drop growth during DWC, known as coalescence. If coalescence does occur, the merging droplets are substituted by a new droplet with a volume equal to the sum of the volumes of the droplets involved in coalescence. The center of mass of the coalescing droplets is calculated to determine the position of the new drop. The criterion for identifying contacting droplets depends on surface wettability. For a hydrophilic surface ($\theta < 90°$), the drops merge at the point where their triple lines overlap, which occurs when the distance separating the centres of mass of drops i and j is less than the sum of their base radii r_b:

$$r_{b,i} + r_{b,j} > \sqrt{\left(x_i - x_j\right)^2 + \left(y_i - y_j\right)^2} \tag{3}$$

where x and y are the coordinates of the droplet centre. On the other hand, for a hydrophobic surface ($\theta > 90°$), the droplets merge when the spacing between the centre of mass of drops i and j becomes smaller than the sum of the curvature radii r of the droplets involved in coalescence. Considering that the coordinates of a droplet are (x, y, $|r \cos\theta|$), the condition that triggers coalescence for hydrophobic surfaces is:

$$r_i + r_j > \sqrt{\left(x_i - x_j\right)^2 + \left(y_i - y_j\right)^2 + \left(r_i - r_j\right)^2 cos^2\theta} \tag{4}$$

The determination of the reciprocal distances between the droplets is the most computationally demanding step. Although N_s is not a limiting factor for simulations of DWC from humid air [8,17,43], optimizing the droplet distance calculation algorithm is crucial for expanding the computational domain area. To address this, the C programming language has been suitably coupled with the MATLAB® OpenMP library, enabling parallel calculation across multiple cores. It should be noted that coalescences are considered instantaneous events in the numerical simulation, implying that merging drops are replaced by new droplets with different sizes and positions within a single time step.

2.3. Droplet motion

Driven by coalescence and direct condensation, droplets continue to grow until they reach the critical size determined by the maximum radius equation developed by Tancon et al. [44,45]. In the absence of drag forces acting on the droplet, the maximum radius r_{max} is the outcome of the balance between capillary and gravity forces, and is expressed as:

$$r_{max} = \left(\frac{6\, k_c\, \sigma sin\theta(cos\theta_r - cos\theta_a)}{\pi(2 - 3cos\theta + cos^3\theta)\rho_l\, g}\right)^{1/2} \tag{5}$$

where θ_a and θ_r are respectively the advancing and receding contact angle, $g = 9.81$ m s^{-2} is the gravity acceleration, and k_c is the retention factor, which is equal to $2/\pi$ for a circular droplet [46].

Upon reaching the maximum size, the droplet begins to move, renewing the underlying surface. Position and velocity of the sliding drop are calculated by the software at each time step. According to the

Tancon et al. [44] observations of droplets sliding with constant acceleration during DWC on a vertical surface, a constant value of 1 m s^{-2} is assumed in the present study. Accounting for droplet acceleration in the numerical simulation distinguishes the present model from Stevens et al. [23], in which the drops disappear when reaching the maximum dimension, and from Lethuillier et al. [24], which employs a fixed velocity value. To track the droplet's centre position throughout its movement, the equation of uniformly accelerated motion is used, as shown below:

$$\Delta y = a(t - t_0)\,\Delta\tau + \frac{1}{2}a\,(\Delta\tau)^2 \tag{6}$$

where $\Delta\tau$ is the time step, a the drop acceleration, t_0 the initial time of the sliding and t the present time in the simulation.

It is noteworthy that the droplet sliding calculated by Eq. 6 represents discrete motion as a function of the time step. Using a too large time step will result in non-swept portion areas along the droplet path. Since the time interval used for the present simulations is in the order of milliseconds (see Section 2.5), it is possible that some drops along the sliding droplet's path may not be swept away, preventing complete surface renewal. To address this numerical issue, a dedicated algorithm was developed to reconstruct the sliding droplet's path after determining its new position. This algorithm enables the detection of any drops not cleared by the moving drop. Subsequently, the volume of the identified drops within the path of the sliding droplet is added to the volume of the sliding droplet.

After each surface cleaning, triggered by either coalescence or sliding events, the IBM checks the availability of any free nucleation site. At the next iteration, a droplet of radius r_{min} is positioned on each available site.

2.4. Output parameters of the simulation

Upon achieving quasi-steady state conditions (as defined by Eq. 8), the simulation terminates, yielding the following key outcomes: the instantaneous and average heat flux, and the average drop-size distribution. At each time step, the software records the dimensions and positions of all droplets within the computational domain plus the instantaneous heat flux. The latter is obtained by calculating the sum of the individual heat flow rate exchanged by all drops present at that time step, as follows:

$$\tilde{q} = \frac{1}{A}\sum_{i=0}^{n} Q_d(r_i) \tag{7}$$

where n is the number of drops over the surface at each time step, A is the area of the computational domain, and Q_d is the heat transfer for a single droplet calculated according to the growth rate model by Zheng et al. [17]. For a fixed set of thermodynamic and geometric parameters, q_d is solely dependent on its radius. At the end of the simulation, the instantaneous heat flux is averaged to determine the mean heat flux. For obtaining the drop-size distribution, the entire radii range between r_{min} (Eq. 1) and r_{max} (Eq. 5) is divided into bins. In this work, the interval has been divided logarithmically into 70 bins. The radii of the drops calculated at each time step are assigned to their respective bins. This process is repeated for all simulated time steps to obtain the frequency. The distribution of drop-size is then evaluated as the frequency divided by the area of the computational domain and by the corresponding bin size to obtain the number of droplets per unit area per radius.

2.5. Effect of numerical inputs

The developed IBM requires two types of inputs: physical/thermodynamic parameters and numerical parameters (Table 1). Physical/thermodynamic inputs encompass characteristics of the humid air, including its temperature (T_{air}) and relative humidity (RH), accommodation coefficient (α), θ_a and θ_r, coating thermal conductivity λ_{HC}, coating thickness δ_{HC}, and nucleation sites density (N_s). Numerical inputs comprise the area of the computational domain (A), the time step of the simulation ($\Delta\tau$) and its duration (Δt).

Table 1
List of input parameters used for the numerical simulations.

Input parameter	Value
Physical/thermodynamic	
T_{air} [°C]	28
RH [%]	70
$\Delta T_{dew\text{-}wall}$ [K]	10
N_s [m^{-2}]	7×10^8
α [−]	0.001 *
δ_{HC} [nm]	200
λ_{HC} [W m^{-1} K^{-1}]	0.2
θ_a [°]	87
θ_r [°]	72
Numerical	
$\Delta\tau$ [s]	From 10^{-3} to 1
A [mm^2]	12.25, 25, 100
Δt [h]	Up to 3

* The accommodation coefficient used in the present analysis is the value suggested by Zheng et al. [17].

The choice of numerical inputs is strongly affected by the operating conditions, particularly N_s. To maintain acceptable calculation times, the maximum number of droplets in the domain (n_{max}) needs to be limited to a few millions. As a result, for a given value of N_s, the maximum computational domain is constrained by the relationship $A_{max} = n_{max} / N_s$. For example, to keep the computational time within reasonable limits for nucleation site densities typical of steam DWC (about 10^{11}–10^{13} m^{-2} [5,43]), the computational domain must necessarily be kept small, around 1 mm^2. Another crucial consideration is that, as the number of droplets increases, the time step must be reduced to avoid excessive coalescence of droplets from one time step to the next. This, in turn, increases the computational time and alters the profile of the drop-size density function below a certain value of droplet radius (see Fig. 2b). Additionally, for a fixed computational time, the smaller the time step, the shorter the simulation time (Δt). Unlike DWC of pure steam, simulating DWC from humid air offers the advantage of requiring lower values of N_s [8], typically below 10^{10} m^{-2}. Consequently, the computational domain can be enlarged and the simulation time extended, allowing an accurate study of the droplet population and heat flux.

The effects of numerical domain size, simulation time step and duration are examined in detail below. Considering the minimal effect of RH and wall subcooling on N_s, an average value of 7×10^8 m^{-2} is assumed for all simulations in this study, consistent with experimental data reported in Tancon et al. [8]. The rest of the input parameters can be found in Table 1.

In the presence of humid air, the droplet growth rate and thus the heat transfer are strongly limited by vapor diffusion. This means that the time required to complete a condensation cycle (from nucleation to sliding) increases considerably compared to pure steam condensation, from about 1 s to hours. Therefore, the time step used to simulate DWC with NCG must be sufficiently large. Fig. 2a depicts the droplet growth rate calculated by the Zheng et al. [17] model plotted against drop radius for various time step values (0.001–1 s). For comparison, a reference droplet growth rate function (in red in Fig. 2a), derived analytically using the equations described in Supplementary Material S3, is also reported.

The shape of the growth rate function obtained using time steps ranging from 0.001 s to 0.01 s perfectly approximates the reference case. However, with increasing time step from 0.1 to 1 s, the simulated droplet growth rate diverges from the analytically calculated function. Consequently, the drop-size distribution determined by the model results distorted in the region of smaller droplets. Indeed, as depicted in Fig. 2b,

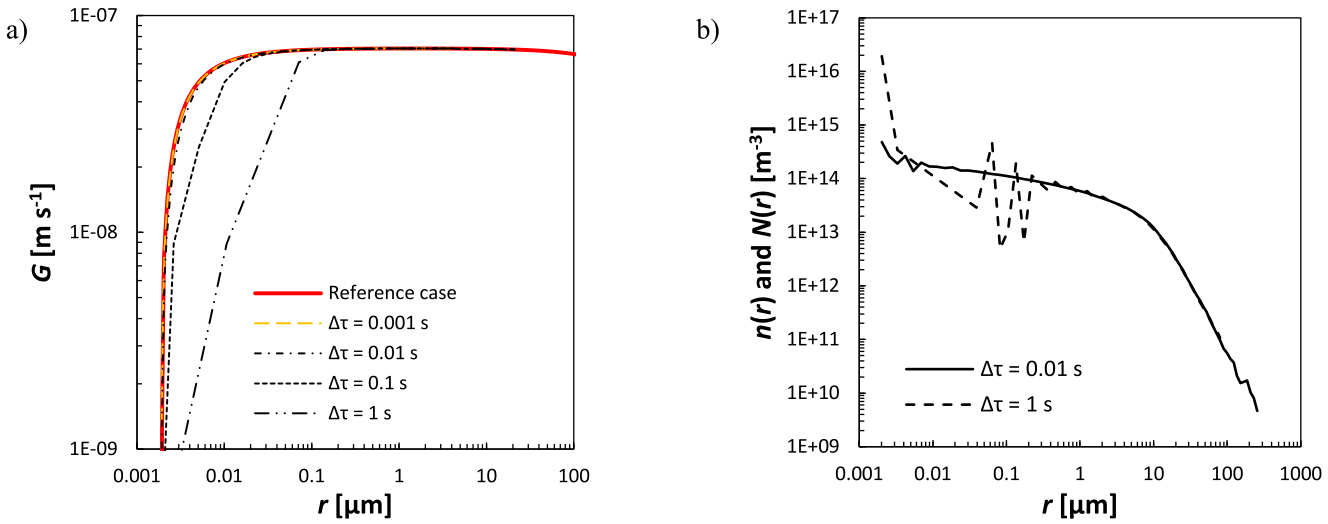

Fig. 2. a) Droplet growth rate G calculated by the Zheng et al. [17] model for different simulation time steps $\Delta\tau$ (between 0.001 and 1 s). b) Drop-size distribution evaluated by the IBM for $\Delta\tau = 0.01$ s and $\Delta\tau = 1$ s. The maximum radius r_{max} is set equal to 300 µm. The other inputs are given in Table 1.

the droplet distribution obtained using a time step of 0.01 s is accurately represented over the whole radius range. The distribution of small droplets does not change with a time step of 0.001 s and overlaps with the distribution derived using 0.01 s. Therefore, only the results obtained with the 0.01 s time step are included in Fig. 2b. In contrast, with a time step of 1 s, the distribution of the small drops ($r < 1$ µm) is not correctly predicted by the IBM, exhibiting an unrealistic scattered behaviour. This is attributed to the fact that smaller drops can grow up to 5 times their size between two consecutive time steps (Fig. 2a). For this analysis, the value of r_{max} was set to 300 µm, a value smaller than that obtained from Eq. 5 (approximately 1 mm), in order to reduce the calculation time. It should be noted that the influence of the time step is negligible for drops with a radius >1 µm.

The accuracy of the simulation results increases with increasing computational domain area. In a larger domain, multiple drops can reach r_{max} simultaneously in different regions of the domain. Additionally, once a drop reaches the critical size, it can travel a greater distance, sweeping the underlying drops before they are able to reach the maximum size. In contrast, in a small domain, a droplet reaching r_{max} cleans a larger portion of the surface, affecting the calculation of heat flux and drop-size distribution. Three simulations with domains of 3.5 × 3.5 mm^2, 5 × 5 mm^2 and 10 × 10 mm^2 were compared in terms of drop-size distribution and average heat flux (q_{cond}). All three simulations were run using the same input parameters (Table 1) until 1 h of simulation time was reached. For average heat flux, the simulation performed with the smallest area (3.5 × 3.5 mm^2) resulted in a relative deviation of 5% from the reference simulation, i.e. the one run with an area of 10 × 10 mm^2. In the case of the intermediate domain (5 × 5 mm^2), the percentage deviation was <1%. Fig. 3a reveals that the drop-size function remains unaffected by the domain size in most of the radius range. However, near r_{max}, the drop-size density function calculated with the smallest domain is affected by the presence of a single large drop at a time. This analysis indicates that both the droplet distribution and average heat flux are adequately described when using a computational domain with a side twice the maximum droplet diameter.

The last numerical parameter to consider is the simulation time Δt. An excessively small value can introduce errors in the calculation of q_{cond}, as shown in Fig. 3b. On the other hand, an excessively long simulation time would be redundant, as the pseudo-cyclic nature of DWC ensures that steady-state conditions are reached after a certain time. This condition can be identified by the convergence of the average heat flux. Therefore, the optimal simulation time should be determined

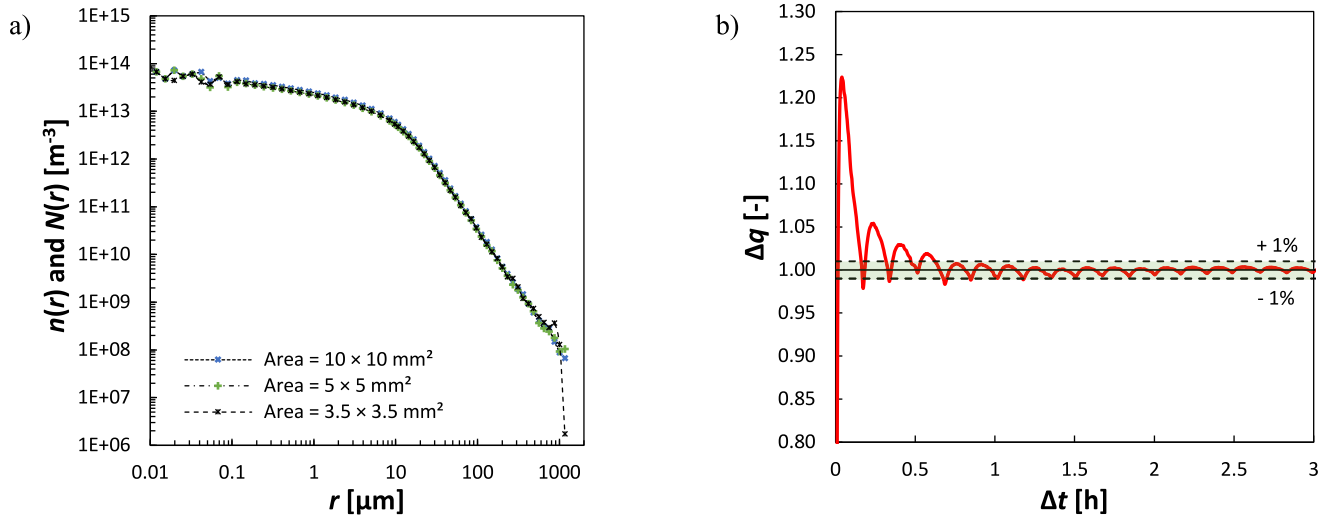

Fig. 3. a) Drop-size distribution vs droplet radius for different computational domain area: 3.5 × 3.5 mm^2, 5 × 5 mm^2 and 10 × 10 mm^2. b) Relative heat flux variation (Eq. 8) vs simulation time Δt.

based on the percentage change in heat flux, calculated using the following equation:

$$\Delta q = \frac{\sum_i \widetilde{q}_i(t)}{q_{cond}} \tag{8}$$

where $\widetilde{q_i}$ is the instantaneous heat flux. If the variation in q_{cond} becomes <1%, the simulation can be considered to have reached steady-state conditions. Fig. 3b shows an example of the calculation of Δq for a simulation iterated up to 3 h. After approximately 1 h of simulation, the change in Δq remains within ±1%, indicating that steady-state conditions have been reached. Therefore, this parameter is monitored throughout the simulation to decide when it can be considered complete.

Based on the previous analyses, the simulations reported in Section 4 will be performed using $\Delta\tau = 10$ ms, which is sufficient to observe the growth of the smallest droplets, a computational domain of about 6 × 6 mm^2, approximately twice the maximum droplet diameter, and a computation time calculated according to Eq. 8.

3. Experimental methods

This section presents the experimental apparatus, data reduction technique, and video acquisition system used to study DWC of humidity present in air. The method adopted here for the experimental evaluation of the droplet growth rate by optical analysis is also discussed in detail. The present experimental data of latent heat flux and drop-size distribution are taken from Tancon et al. [8]. Instead, the optical measurements used to determine the droplet growth rate represent new data not previously published.

3.1. Thermal measurements

Condensation was studied on an aluminum sample (condensing area equal to 40 × 40 mm^2) functionalized by a hybrid silica-based coating deposited by sol-gel method [47,48]. After functionalization, the sample was nearly hydrophobic ($\theta_a = 87° \pm 3°$ and $\theta_r = 72° \pm 2°$). A coating thickness of 200 nm was evaluated by ellipsometry. Further details on surface fabrication and characterization are available in Supplementary Material S3 and in Tancon et al. [8].

The apparatus used to perform condensation tests is composed of a closed circuit with two main parts: an environmental chamber and a test chamber (Fig. 4a-b). Briefly, the environmental chamber controls the thermodynamic conditions of the humid air, then two variable speed fans drive the airflow through an insulated pipe into the test chamber. Enclosed within a transparent channel, the test section accommodates the aluminum specimen upon which the moisture condenses (Fig. 4c). Condensation is induced by a Peltier module positioned on the opposite side of the test section with respect to the sample. The conditioned airflow is then redirected to the environmental chamber through a second insulated pipe, closing the loop. Thermal insulation of all components prevents heat dissipation to the surroundings.

The condensation heat flux is determined by measuring the mass of condensate using a laboratory scale. The test section is hung on the scale, enabling continuous monitoring of the total mass of condensate collected on the sample and in the water tank. From the average condensate mass flow rate (m_{cond}) obtained from the time derivative of the scale measurement over the entire duration of the test (100 min), the average condensation heat flux is calculated as:

$$q_{cond} = \frac{m_{cond}\,\Delta h_{lv}}{A_{cond}} \tag{9}$$

where A_{cond} is the sample area (40 mm × 40 mm) and Δh_{lv} is latent heat evaluated at T_{wall}. Given the expected low heat flux values during condensation from moist air (< 1400 W m^{-2}) and the experimental uncertainty on the temperature reading (± 0.05 K) [8], it can be assumed that the temperature difference across the 2.5 mm aluminum thickness between the sensor position and the condensing surface is negligible. Consequently, the surface temperature (T_{wall}) can be directly

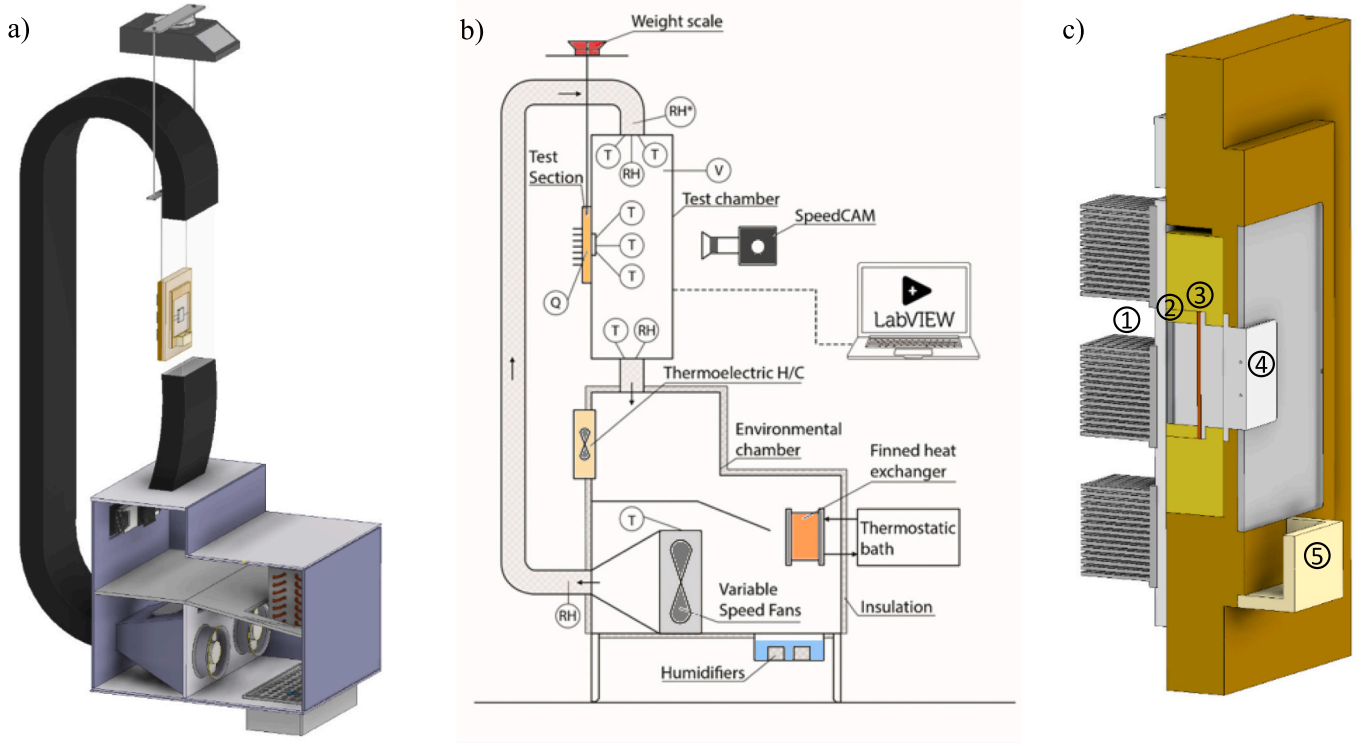

Fig. 4. a) 3D model and b) layout of the test rig with the position of the main elements highlighted. c) Cross-sectional view of the test section: (1) heat sink, (2) Peltier module, (3) heat flux sensor, (4) sample, (5) water collector.

Table 2
Operating conditions for condensation tests.

Parameter	Value
T_{air} [°C]	28
RH [%]	50, 70, 90
x_{air} [kg_v/kg_{dryair}]	0.012, 0.017, 0.022
$\Delta T_{dew\text{-}wall}$ [K]	7, 10, 13
v_{air} [m s^{-1}]	1

obtained by averaging the readings of two Pt-100 transducers inserted into the specimen. A chilled-mirror hygrometer is employed to directly detect the dew point (T_{dew}) at the inlet of the transparent channel. The airflow temperature is evaluated as the average of two Pt-100 readings at the entrance and exit of the channel. Fluid properties are determined with REFPROP v10 [42].

In Table 2, the range of the operating conditions is reported. In particular, the experimental data refer to an air temperature of 28 °C and relative humidity in the range 50–90%, which correspond to specific humidity (moisture content, x_a, defined as the ratio of the mass of vapor to the mass of dry air in a given volume of humid air) between 0.012 and 0.022 kg_v/kg_{dryair}. The experiments were conducted under steady-state conditions, ensuring that all operating conditions remained constant throughout each test session. During these tests, the condensate mass was measured to determine the latent heat flux exchanged by the sample. Each experimental point presented in this paper represents the average of 20 distinct data sets, collected at 5-min intervals. Each data set comprises 30 readings obtained over 60 s of continuous acquisition. To establish a representative value, the mean value of each data set was calculated. Uncertainty analysis was performed in compliance with the ISO guide [49]. All expanded uncertainties were calculated with a coverage factor $k = 2$. Within the investigated range of operating condition, the uncertainty associated with condensation heat flux (Eq. 9) remains always below 2%. For further information on the test apparatus, experimental procedure, data reduction, and experimental uncertainties, please refer to Supplementary Material S4 and Tancon et al. [8].

3.2. Optical measurements

A high-speed camera with a CMOS sensor consisting of 1280 × 1024 pixel array is employed to visualize the DWC phenomenon. Each video is recorded at 0.5 fps after the sample surface has been dried to ensure measurement repeatability. For clear detection of droplet contours, ring-shaped illumination is used. The camera can be equipped with either a macroscopic lens or a microscopic lens, providing image magnification up to 7 times. The choice of lens depends on the specific purpose of the analysis.

To characterize the population of drops and evaluate the drop-size distribution, recorded videos were analysed with a custom-developed MATLAB® software, specifically trained to detect the actual dimension of droplets based on the ring of light reflected on their surface. Once the program's input parameters are optimized, each video frame is analysed through a series of stages to evaluate the size and position of each ring of reflected light. Then, the light ring recognised by the program is resized using an appropriate calibration function to determine the real drop size. These stages are repeated iteratively for the complete sequence of video frame, allowing the evaluation of the drop-size distribution. For further details regarding the program's functionality and implementation, please refer to [3,45].

To investigate droplet growth rate (G), only microscopic videos were utilized to detect drops with radii ranging from approximately 5 to 300 μm. Prior to determining the experimental growth rate of a specific droplet, the interval of video frames in which it primarily grows by direct condensation (without any discernible coalescence with other droplets) must first be identified. Then, a custom MATLAB® program is used to evaluate droplet diameter over time (Fig. 5a). As depicted in Fig. 5b, the droplet growth within the identified time interval follows a linear trend. To calculate the growth rate of the droplet ($G = dr/dt$), data have been fitted with a linear function and the slope of the interpolating line is calculated according to the least squares method as follows:

$$G = \frac{N\sum(t_i r_i) - \sum t_i \sum r_i}{N\sum t_i^2 - (\sum t_i)^2} \tag{10}$$

where N is the number of frames considered for the calculation of the growth rate and r_i is the radius of the droplet measured at the instant t_i. This calculated growth rate is associated with an average droplet radius r between the first and last frames analysed by the program. Finally, to determine the average droplet growth rate as a function of the radius, 30 to 50 droplets were analysed for each operating condition.

4. Results and discussion

In this section, measurements of droplet growth rate are used to identify the most accurate model for predicting the heat exchanged by an individual droplet among those considered in Section 2.2. The selected model is then integrated in the present IBM to perform simulations of DWC from moist air at varying relative humidity and dew-to-wall temperature difference. For validation purposes, the numerical results are compared against experimental data taken from our previous work [8], both in terms of condensation heat flux and distribution of drop-size. Finally, the developed IBM is employed to numerically assess the effect of operating conditions, accommodation coefficient and surface wettability on DWC.

4.1. Choice of heat transfer through a single droplet model

All models considered in Section 2.2, except for Suzzi and Croce [32], depends on the accommodation coefficient (see Supplementary Material S2 for the equations). This coefficient remains the only input parameter that lacks experimental determination and, thus, is typically assumed. As previously discussed in the Introduction, due to the complexity of direct measurements of α, a broad range of values is reported in the literature, spanning from 1 to 10^{-5} [26,27]. This lack of knowledge about α also complicates the choice of a model for q_d. Hereafter, we want to use measurements of drop growth rate to infer the value of α that yields the best fit for each model to the experimental data. Then, the model for heat transfer trough a single drop to be coupled with the developed IBM is selected based on the minimum deviation between numerical and experimental values.

Using the method described in Section 3.2, the videos recorded during DWC on the coated surface were analysed to estimate the droplet growth rate at varying operating conditions. Fig. 6a shows the values of growth rate measured at varying RH (50, 70, 90%) plotted versus average droplet radius for a constant $\Delta T_{dew\text{-}wall}$ (10K), air velocity (1 m s^{-1}), and air temperature (28 °C). For a fixed radius, an increase in air humidity results in a corresponding increase in droplet growth rate (Fig. 6a). On average, the droplet growth rate at RH = 90% is 76% higher than the values obtained at RH = 50%. Although the uncertainties in the growth rate evaluation are significant (the mean deviation is around 25%), these measurements clearly identify the trend and order of magnitude of the experimental droplet growth rate under the considered operating conditions.

As a next step, the four models for heat transfer through a single droplet (Zheng et al. [17], Baghel et al. [18], Lyu et al. [19] and Suzzi and Croce [32]) were used to predict the experimental data of droplet growth rate. To compare the analytical and experimental growth rates, the standard deviation was evaluated when varying α. The procedure involves setting a specific accommodation coefficient between 10^{-3} and 10^{-5} (20 discrete values within the specified range were considered). The deviation between the experimental values and the analytical

models is then calculated, assuming that the accommodation coefficient remains constant in the whole range of operating conditions here considered. This procedure was applied to the models of Zheng et al. [17], Lyu et al. [19] and Baghel et al. [18], which included the accommodation coefficient in their modeling, while Suzzi and Croce [32] can be implemented without it. For each model, a single optimal value of α was determined that minimized the mean deviation from the measurements shown in Fig. 6a. This method yielded the following values: $\alpha = 10^{-4}$ for Zheng et al. [17], $\alpha = 9 \times 10^{-5}$ both for Baghel et al. [18], and for Lyu et al. [19]. Due to the assumption of the Suzzi and Croce [32] model, which relies solely on vapor diffusion to calculate the droplet growth rate, no accommodation coefficient is needed for this model. Instead, it is important to note that this model includes two correction parameters to account for the interaction between the droplets and for the actual droplet contact angle. Further details regarding this model can be found in the Supplementary Material S2. Fig. 6b shows the box plot of the ratio between the experimental growth rate taken at different relative humidity (50–90%) and the values predicted by the various models considering the aforementioned values of α. Box plots are a helpful tool in situations where data is not normally distributed. This is because they display the quartiles of the data through a box, while the whiskers demonstrate the remaining distribution. The deviations and statistical distributions of the dataset are easily reflected in the box plot, where large deviations indicate the largest difference in the prediction of droplet growth rate. Fig. 6b clearly show that the Zheng et al. [17] model with an accommodation coefficient of 10^{-4} yields the minimum average deviation (about 22%) from the experimental data. On the other hand, the predictions of the other three models are less accurate, with an average deviation of 32% in the case of Baghel et al. [18] and Lyu et al. [19], and 54% for Suzzi and Croce [32]. Therefore, the Zheng et al. [17] model emerges as the best choice for accurately predicting droplet growth during DWC from humid air. Hence, it will be integrated with the present IBM (Section 2) to perform the simulations reported in the following sections.

4.2. Comparison against experimental data

To assess the proposed IBM, a series of simulations were conducted employing the Zheng et al. [17] model for droplet growth with $\alpha = 10^{-4}$. The numerical results were compared against the measurements of average latent heat flux and drop-size distribution obtained by Tancon et al. [8]. The comparison refers to a fixed air temperature (28 °C), and

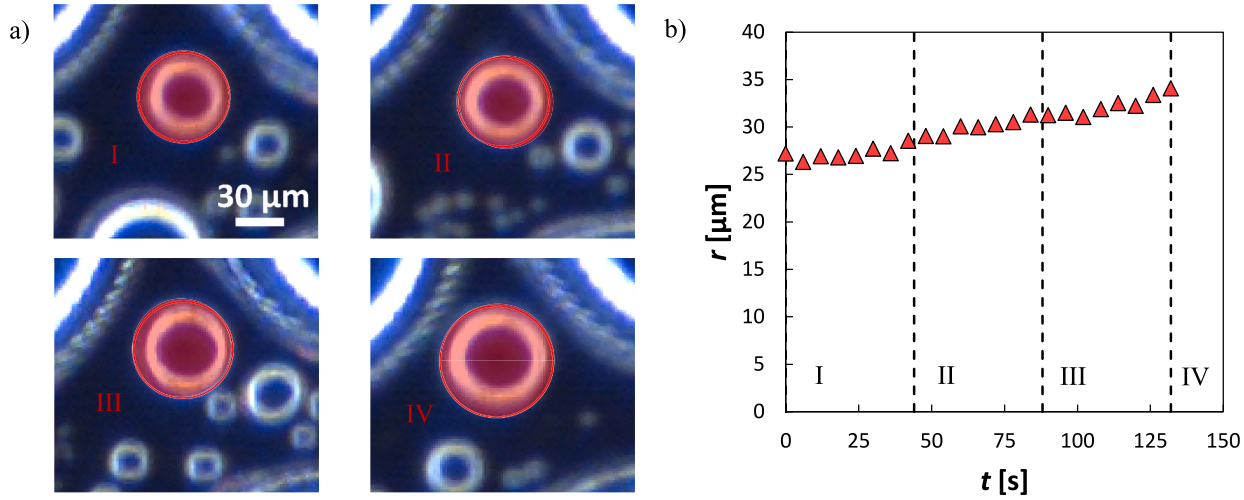

Fig. 5. Example of video analysis for the evaluation of droplet growth rate. a) Images of a drop that grows mainly by direct condensation (at $T_{air} = 28$ °C, RH = 70%, $\Delta T_{dew\text{-}wall} = 10$ K) at four different times: I) 0 s, II) 44 s, III) 88 s, and IV) 130 s. b) Droplet radius over time obtained from the videos using a home-made MATLAB® program.

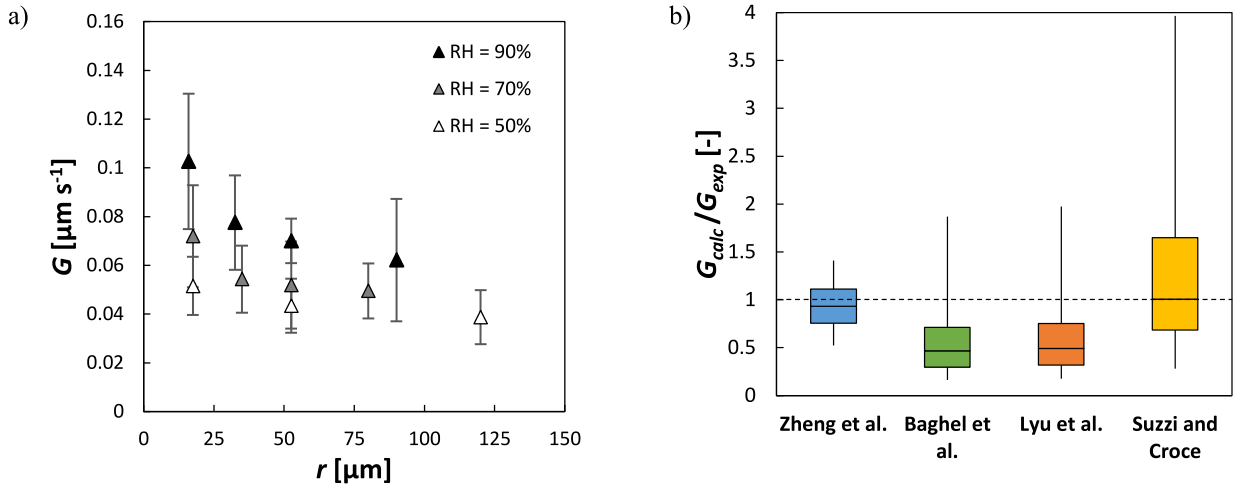

Fig. 6. a) Droplet growth rate measured at different relative humidity (RH = 50–90%) and fixed dew-to-wall temperature difference ($\Delta T_{dew\text{-}wall} = 10$ K) versus average radius. b) Box plot of the ratio between calculated and experimental growth rate obtained at varying RH: values predicted by the Zheng et al. [17], Baghel et al. [18], Lyu et al. [19] and Suzzi and Croce [32] models. The inputs to the model are listed in Table 3.

Table 3
Input parameters for the numerical simulations.

Parameter	Value	Parameter	Value
T_{air} [°C]	28	λ_{HC} [W m^{-1} K^{-1}]	0.2
RH [%]	50, 70, 90	θ_a [°]	87
$\Delta T_{dew\text{-}wall}$ [K]	7, 10, 13	θ_r [°]	72
N_s [m^{-2}]	7×10^8	$\Delta\tau$ [ms]	10
α [−]	0.0001	A [mm^2]	36
δ_{HC} [nm]	200	Δt [h]	Eq. 8

varying RH (50–90%) and $\Delta T_{dew\text{-}wall}$ (7–13 K). The comparison is limited to $\Delta T_{dew\text{-}wall} = 13$ K because the data set for higher values of dew-to-wall temperature difference does not cover all the three RH values. A total of 9 different operating conditions were considered for the validation. The other model inputs are summarized in Table 3.

Fig. 7a shows the average q_{cond} predicted by the present model compared with the experimental data collected during DWC from humid air. The IBM results in excellent agreement with the measurements for all operating conditions, with an average deviation from experimental data of about 4%. In Fig. 7b-c, the instantaneous $\widetilde{q_{cond}}$ and average q_{cond} calculated using the present IBM are compared with the measurements at two RH (70%, 90%) for the same $\Delta T_{dew\text{-}wall}$ (10 K). The instantaneous heat flux $\widetilde{q_{cond}}$ reveals the quasi-cyclic nature of DWC. The simultaneous occurrence of nucleation, droplet growth by both direct condensation and coalescence, and sliding events causes the instantaneous heat flux to oscillate. However, after a transient period of about 10 min at the beginning of the simulation, the pseudo-steady state is reached, and the instantaneous heat flux (blue line) starts to fluctuate around the average value (red dashed line). The presence of sliding events occurring on the surface (e.g., at 70 min in Fig. 7b) is indicated by sudden reductions of the heat flux, as well as coalescence events among big drops (e.g., at 50 min in Fig. 7b). As discussed at the end of Section 2.5, after about 1 h of simulation, the fluctuations in $\widetilde{q_{cond}}$ no longer affect the average heat flux, indicating that quasi-steady conditions have been reached and the simulation can be stopped. At RH = 70%, q_{cond} calculated by the IBM deviates by 6% from the experimental data, whereas the deviation is lower than 1% at RH = 90%. The results in Fig. 7 suggest that the present IBM coupled with the model proposed by Zheng et al. [17] is an excellent tool for predicting the effect of RH and dew-to-wall temperature difference on the latent heat flux during DWC from moist air.

In addition to assessing the average heat flux predictions, validating the calculated drop-size distribution is equally critical. Fig. 8a presents a comparison between the distribution obtained from the IBM and the distribution measured as described in Section 3.2. Due to optical limitations of the measurement system [3,8], the experimental distribution is restricted to radii above 2 μm. The calculated distribution using the Le Fevre and Rose [14] model and the equivalent radius r_e obtained as suggested by Miljkovic et al. [12] are also reported. The latter is usually considered by analytical models as the threshold value between the population of small droplets (on the left) growing by direct condensation and the population of large drops (on the right) growing mostly by coalescence. Fig. 8a demonstrates that the experimental distribution is well approximated in the entire range of radii by the simulation results. Both the numerical and experimental distributions exhibit a decreasing trend with increasing radius, with minimal effects of RH and $\Delta T_{dew\text{-}wall}$. Above r_e, both distributions follow the Le Fevre and Rose [14] trend. Below r_e, the downward trend is less pronounced. It should be noted that the density of drops with radius from r_e to ~20 μm is overestimated by the analytical model compared to the simulation. Since these drops are responsible for a small but non-negligible share (6%) of the total q_{cond} transferred during DWC with humid air (Fig. 8b), employing population-based models for latent heat flux calculations (Supplementary Material S5) could result in overestimations compared to the IBM. Another important finding reported in Fig. 8a is that the distribution of drops appears be unaffected by the thermodynamic conditions of the humid air. Specifically, this result contributes to fill the gap in the literature regarding the shape of the small droplet distribution during DWC with humid air.

To conclude this section, we want to assess the contribution of small droplets ($r < r_e$) to the total latent heat flux exchanged during DWC in presence of humid air. Fig. 8b shows the distribution of the cumulative normalized heat flux (U) plotted against the drop radius r at varying RH and dew-to-wall temperature difference, where U is defined as:

$$U = \frac{\sum_{i=r_{min}}^{r_{max}} \left(Q_{d,i}\, N_i\, \Delta r_i\right)}{q_{cond}} \tag{11}$$

where $Q_{d,i}$ is the heat flowrate transferred trough an individual droplet, N_i is the drop-size distribution, Δr_i corresponds to the radii bin size. The droplet population is divided into several bins (as reported in Section 2.4) from r_{min} to r_{max}, and $Q_{d,i}$ is calculated for each bin. This value is subsequently divided by the total latent heat flux (q_{cond}). On average, the percentage of heat flux due to droplets with a radius smaller than r_e, is <5%. This result is consistent with the suggestion by Zheng et al. [17] to exclude the contribution of small drops from estimations of q_{cond}.

Supplementary Material S5 presents a comparison of latent heat fluxes calculated by the four models using the PBM approach. In fact, as an alternative to numerical simulations, the results shown in Fig. 8b suggest that q_{cond} can be calculated (with satisfactory accuracy) by coupling a model for the heat flux through a single droplet with the Le Fevre and Rose [14] equation for the drop-size density of large droplets, considering only the interval of radii from r_e to r_{max}. While the PBM approach exhibits lower accuracy in predicting the average q_{cond} compared to the simulation-based approach, it offers significantly reduced computational times. Therefore, this approach can serve as a viable alternative to IBM when the primary focus lies in estimating the average thermal performance and temporal evolution of heat flux and droplet population are not essential.

The comparison of the four different models using the PBM approach identify the Zheng et al. [17] model as the most accurate for predicting the effect of RH and $\Delta T_{dew\text{-}wall}$ during DWC from humid air. The average deviation between predicted and experimental values was below 10%; as shown in Fig. 7a, when coupled with the present IBM, Zheng et al. [17] leads to more accurate predictions (mean deviation of 4%). In contrast, the Lyu et al. [19] and Baghel et al. [18] models overestimate the latent heat flux by an average of 30% at RH = 90%, while the experimental data at RH = 50% are underestimated by about 60%. The Suzzi and Croce [32] model performs even worse, with an average deviation of 250% from the experimental data. This is likely due to the strong assumption of this model, which considers the process to be driven solely by diffusion, with the presence of two correction factors.

As demonstrated so far, the use of an IBM enables the underlying mechanisms of the humid air DWC process to be investigated without recourse to simplifying assumptions regarding the drop-size distribution. Furthermore, the IBM provides insights into the dynamic evolution of the drop population and its effect on the instantaneous heat flux, in addition to the average behaviour. In contrast, the PBM requires a model for the drop-size density distribution and it yields only average results. To the best of the authors' knowledge, no specific expressions for the droplet population in the presence of humid air are available in the literature.

4.3. Effect of the accommodation coefficient

This section aims to clarify the dependence of the developed IBM (coupled with the model by Zheng et al. [17]) from the value of α chosen as model input. Section 4.1 revealed that an accommodation coefficient of 10^{-4} minimizes the deviation between calculated and experimental droplet growth rates. To investigate the effect of α on both heat flux and drop-size distribution, numerical simulations were conducted using the present IBM (Section 2) at varying accommodation coefficients (α =

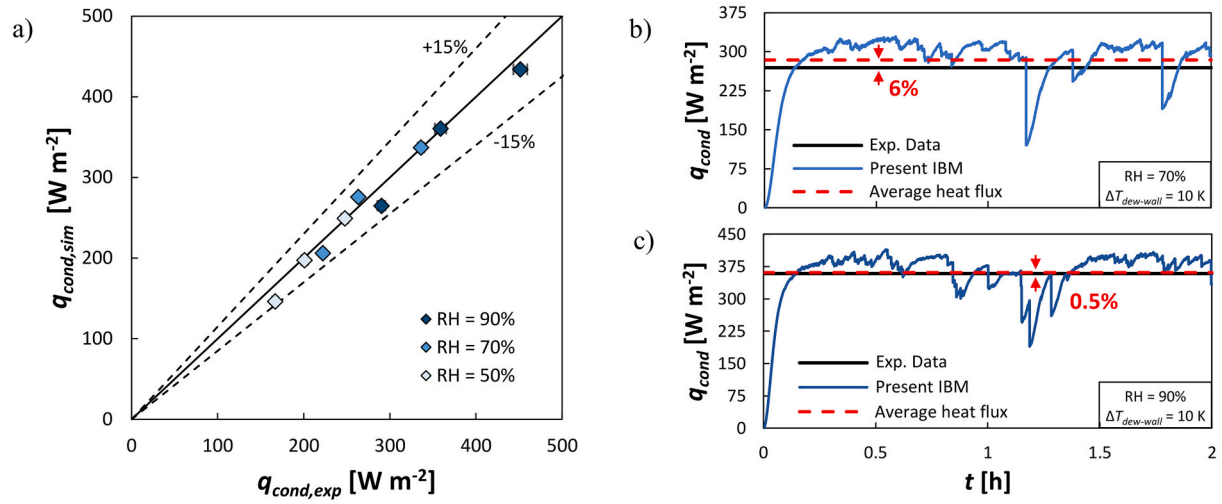

Fig. 7. a) Comparison between the latent heat flux measurements $q_{cond,exp}$ obtained by Tancon et al. [8] and the numerical heat flux $q_{cond,sim}$ predicted by the IBM coupled with Zheng et al. [17]. The experimental data refer to RH = 50–90% and $\Delta T_{dew\text{-}wall}$ = 7–13 K. The other inputs are listed in Table 3. b, c) Instantaneous and average heat flux evaluated by the IBM compared with data obtained at RH = 70%, 90% and $\Delta T_{dew\text{-}wall}$ = 10 K.

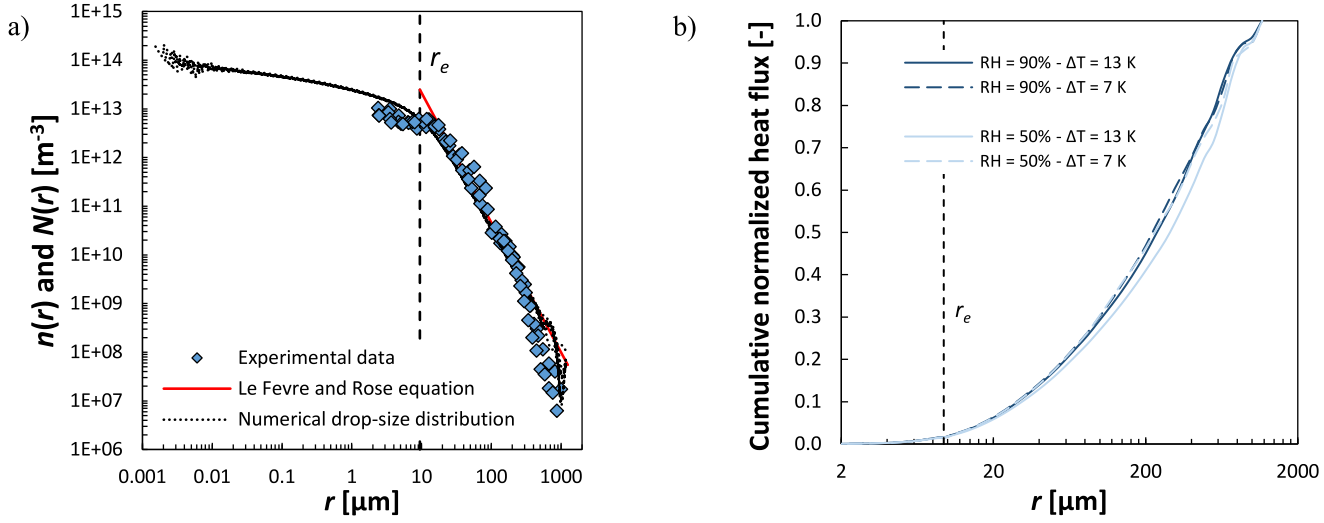

Fig. 8. a) Experimental drop-size distribution compared against the one computed by the IBM for different operating conditions (RH = 50–90%, $\Delta T_{dew\text{-}wall}$ = 7–13 K) versus droplet radius. The calculated distribution of large drops by the Le Fevre and Rose [14] model (r_{max} = 1.44 mm) and the radius r_e evaluated as suggested by Miljkovic et al. [12] are also depicted. b) Cumulative normalized heat flux distribution vs drop radius calculated at different RH and $\Delta T_{dew\text{-}wall}$. The model inputs are listed in Table 3. (For interpretation of the references to colour in this figure legend, the reader is referred to the web version of this article.)

10^{-3}, 5×10^{-4}, 10^{-5}), while keeping constant the numerical inputs ($\Delta\tau = 10^{-2}$, Δt = 2 h), thermodynamic conditions (RH = 70%, $\Delta T_{dew\text{-}wall}$ = 10 K), and nucleation sites density ($N_s = 7 \times 10^8$ m^{-2}). The inputs required for the model operation are summarized in Table 3.

Fig. 9a compares the average latent heat flux obtained by numerical simulations with the experimental value (270 W m^{-2}). An accommodation coefficient $\alpha = 10^{-4}$, which was inferred experimentally, allows to obtain the minimum error (6%) between the experimental data and the results of the numerical simulation. As the accommodation coefficient varies from 10^{-4} to 10^{-3}, the latent heat flux calculated by the IBM increases exponentially, deviating from the measurement. For α equal to 10^{-3}, the relative deviation between numerical prediction and experimental data exceeds 450%. On the contrary, when α is set to 10^{-5}, the predicted value is 85% lower than the experimental data. Fig. 9b shows that the distribution of small droplets remains relatively unaffected by the accommodation coefficient, but it affects the latent heat flux (Fig. 9a). This suggests that α affects the growth rate of individual drops rather than the average drop-size distribution and this result confirms the procedure followed in Section 4.1 where the accommodation coefficient was selected based on the experimental growth rate of single droplets.

It is worth noting that, for droplet radii below 0.1 μm, values of $\alpha > 10^{-4}$ result in a scattered small droplet distribution. This scattering arises from the increased droplet growth rate, which causes these droplets to grow rapidly between two consecutive time steps, altering the shape of the function describing the drop-size distribution. Reducing the time step used for the simulations would eliminate this scattering, further demonstrating that the effect of α on the distribution of drop-size is negligible over the entire range of droplet radii.

Data in Fig. 9 showed that an increase in the accommodation coefficient leads to a significant increase in the droplet growth rate, making the DWC mechanisms faster and improving q_{cond}. Conversely, a reduction of α results in a longer time required to complete a DWC cycle. To further validate the value of the chosen accommodation coefficient, the experimental evolution of droplet population can be qualitatively compared with the simulated one. Fig. 10 presents a direct comparison

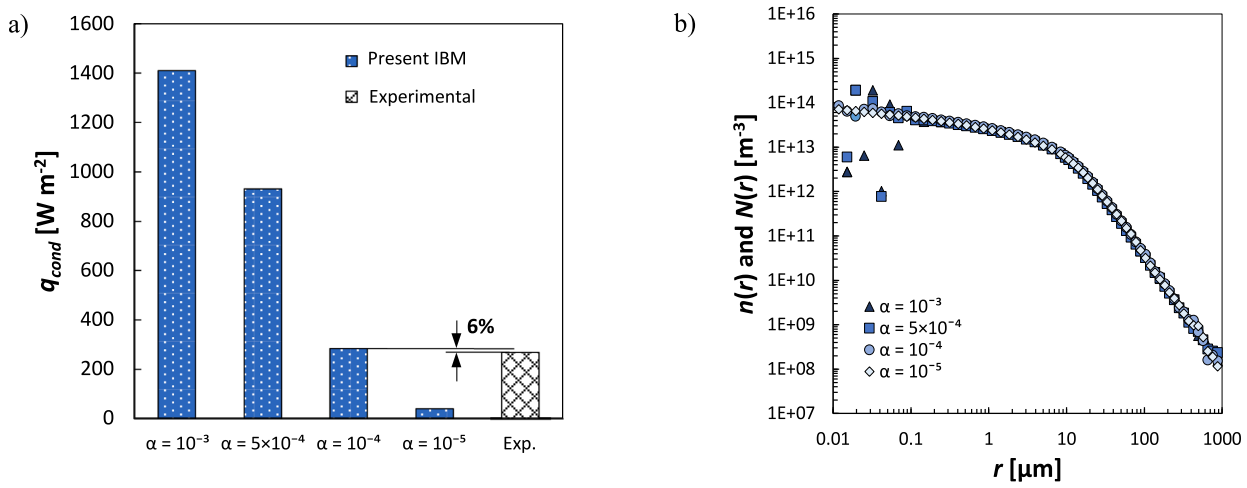

Fig. 9. a) Average q_{cond} predicted by the developed model (Section 2) for varying α compared with the experimental value at RH = 70% and $\Delta T_{dew\text{-}wall} = 10$ K. The relative deviation between the numerical result obtained with $\alpha = 10^{-4}$ and the measurement is also reported. b) Drop-size distribution vs drop radius at varying α. Input values are listed in Table 3.

between the evolution of droplet population obtained from simulations and from the experimental observation during DWC at RH = 70% and $\Delta T_{dew\text{-}wall} = 10$ K. In Fig. 10a, the evolution of the condensation process is shown at three successive time-steps ($t = 0$, 10, 20 min). The images were taken in the central region of the condensing surface using a microscope objective, allowing the analysis of an area of approximately 1.5×1.5 mm^2, as described in Section 3.2. The comparison between the simulated trend and the actual observation demonstrates a remarkable agreement with the droplet sizes observed at the same time. Fig. 10b compares the experimental growth of a single droplet with that simulated with the present IBM. The experimental data, obtained by tracking the size of a marked droplet (red circles) as it grows due to direct condensation and coalescence, is well-matched by the simulation. During the first 5 min, the simulation accurately predicts the droplet growth which is dominated by direct condensation. As coalescence becomes more dominant ($t > 8$ min), the growth of both the experimental droplet and the simulated droplet become asynchronous. However, the dimensions predicted by the simulation remain in close agreement with the experimental evolution, even after coalescence. The accurate prediction of the droplet evolution provided by the simulation provides convincing evidence in support of the chosen accommodation coefficient ($\alpha = 10^{-4}$).

4.4. Effect of surface wettability

The analyses carried out in Sections 4.2–4.3 indicate that the drop-size distribution is influenced neither by the operating conditions of humid air (relative humidity and surface subcooling) nor by the accommodation coefficient. On the other hand, these parameters do affect the droplet growth rate and, thus, the condensation heat flux. At this point, it only remains to elucidate the effect of surface wettability, defined by the equilibrium contact angle ($\theta_e = \cos^{-1}(0.5\cos\theta_a + 0.5\cos\theta_r)$). The developed IBM coupled with the model by Zheng et al. [17] is used here to perform numerical simulations for three different surface wettabilities: hydrophobic with $\theta_e = 120°$, baseline nearly hydrophobic with $\theta_e = 77°$ and hydrophilic with $\theta_e = 45°$. The contact angle hysteresis

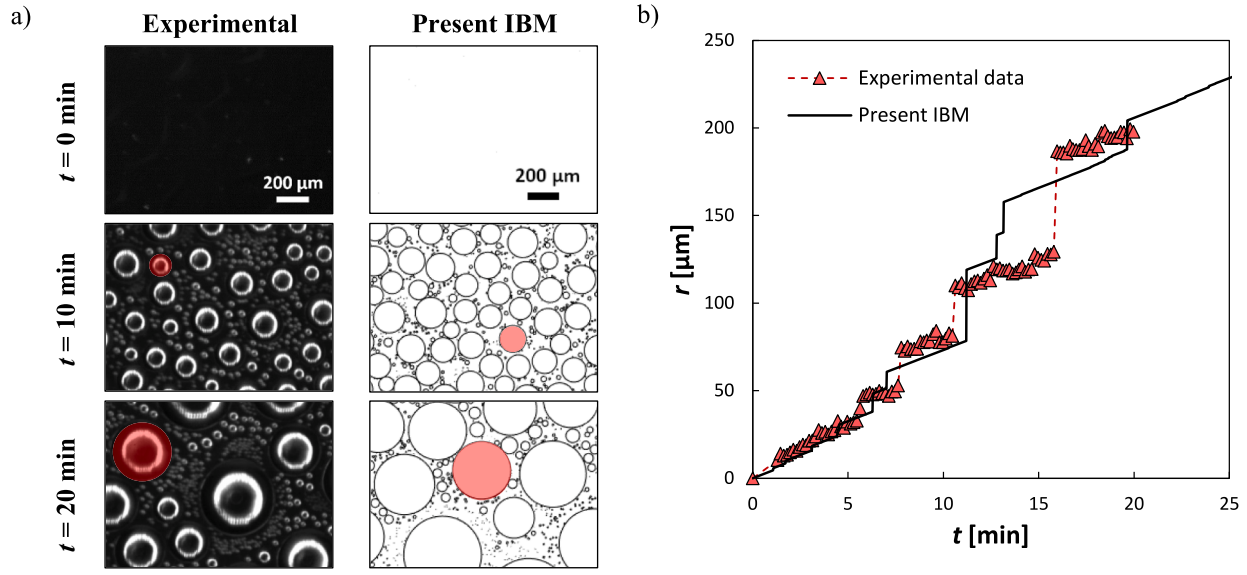

Fig. 10. a) Experimental and simulated (by the present IBM coupled with the model of Zheng et al. [17]) evolution of condensation from moist air. b) Comparison of the simulated and experimental droplet growth due to both direct condensation and coalescence. Both the simulation results and video frames refer to the same experimental conditions ($T_{air} = 28$ °C, RH = 70%, $\Delta T_{dew\text{-}wall} = 10$ K). The numerical inputs are $N_s = 7 \times 10^8$ m^{-2}, $\Delta\tau = 0.01$ s and $\alpha = 10^{-4}$. The visualized area and computational domain both measure 1.5×1.5 mm^2.

was maintained constant at 20°, while the departing radius was calculated by Eq. 5. The operating conditions common to all simulations were RH = 70%, $\Delta T_{dew\text{-}wall}$ = 10 K, and T_{air} = 28 °C. The accommodation coefficient was fixed at 10^{-4}. The other input values are listed in Table 3.

Fig. 11 shows the drop-size distribution, the heat flux through a single droplet and the average q_{cond} calculated from numerical simulation for the three wettabilities. Fig. 11a depicts the drop-size distribution plotted against drop radius, revealing a notable difference in the density of small drops across the three surface wettabilities. The hydrophobic surface ($\theta_e = 120°$) exhibits a higher density of small drops compared to the baseline (θ_e = 77°) and hydrophilic (θ_e = 45°) surfaces. Since θ_e varies while the contact angle hysteresis is fixed, the calculated departing radius r_{max} differs significantly between the hydrophilic surface (2.5 mm) and the hydrophobic surface (0.8 mm). Despite this difference, the distribution of large drops does not seem to be affected by these variations in r_{max}. Thus, it appears that the distribution of small droplets during DWC from humid air is affected only by the surface wettability, whereas that of large drops exhibits a negligible dependence from r_{max}, thus much weaker than suggested by Le Fevre and Rose [14]. In contrast to the results obtained when studying DWC of pure steam [16], here the drop-size distribution function is insensitive to the departing radius in the examined range (0.8–2.5 mm). However, the heat transfer performance is not likely to be significantly affected by the higher density of small drops on the hydrophobic surface (Fig. 11a), as the contribution of drops with a radius smaller than 10 μm to the total heat flux is almost negligible (Fig. 8b). On the other hand, the surface wettability strongly affects the heat transferred though a single droplet (Fig. 11b). Focusing on the droplet radii range from 10 μm to r_{max}, which contributes the most to the average condensation heat transfer (> 95%) according to the results shown in Fig. 8b, an increase in contact angle from 77° to 120° leads to an increase of about 110% in the heat flux though a single droplet. Instead, a reduction in contact angle from 77° to 45° results in an average q_d reduction of 23%. Mainly due to this effect on the heat transfer through a single droplet, the reduction in surface wettability significantly enhances the average q_{cond} (Fig. 11c), from 270 W m^{-2} at θ_e = 77° to 540 W m^{-2} at θ_e = 120° (100% increase). It should be noted that, on the hydrophobic surface, the droplets also exhibit increased mobility and reduced average size, resulting in improved surface renewal. Conversely, the decrease in contact angle from 77° to 45° leads to a decrease of about 33% in the average latent heat flux (Fig. 11c). The decrease in latent heat flux on the hydrophilic surface is primarily due to a reduction in heat transfer by individual droplets. Additionally, the increase in average droplet size and r_{max} results in the formation of a few large droplets with high conduction resistance on the computational domain.

5. Conclusions

This work introduced a novel individual-based model (IBM), implemented in hybrid MATLAB® and C programming languages, for simulating dropwise condensation in humid air conditions. Experimental measurements were used to choose the droplet growth rate model among those considered (Zheng et al. [17], Suzzi and Croce [32], Lyu et al. [19], and Baghel et al. [18]) and to assess the accuracy of the developed IBM. Then, the numerical model was employed to investigate the small drop population. The key findings are listed below.

- An efficient individual-based model (IBM) developed to track the growth of each droplet on the condensing surface was developed to simulate the DWC phenomenon in presence of moist air. The use of the OpenMP library allowed the simulation to be parallelized on 32 threads, significantly reducing the computation time and increasing the computational domain area and the simulation duration, achieving a comparison with experimental data without numerical limitations.
- Compared to the population-based approach, the IBM offers several advantages. Specifically, it does not require the assumption of a model for the drop-size distribution, allowing for direct comparison of various single-drop heat transfer models with measured data. Furthermore, the IBM provides insights into the dynamic evolution of the drop population and its effect on the instantaneous heat flux, in addition to average behaviour.
- The growth rate of drops with radii between 10 and 125 μm was measured by analyzing the videos recorded during condensation from humid air using a custom MATLAB® code for tracking drop growth. When the relative humidity varied from 50% to 90%, the droplet growth rate increased by about 76%. From the comparison against experimental data, the Zheng et al. [17] model assuming an accommodation coefficient of 10^{-4} emerged as the best choice for accurately predicting droplet growth during DWC from humid air.
- The present numerical simulations were validated with measurements of latent heat flux and drop-size distribution obtained from Tancon et al. [8] at varying relative humidity (50–90%) and dew-to-wall temperature difference (7–13 K). The agreement between calculated and experimental values (within 6%) suggests that the present IBM coupled with the model by Zheng et al. [17] for droplet growth rate is an excellent tool for predicting the effect of relative humidity and dew-to-wall temperature difference on DWC in the presence of humid air.
- After validation, the developed IBM was used to get insight into the distribution of small droplets during condensation of moisture from humid air. Numerical simulations revealed that the contributions of drops with r < 10 μm to the total heat flux during DWC is <5%. Furthermore, it was found that the drop-size distribution is almost independent from surface subcooling, relative humidity, and accommodation coefficient, whereas it is affected by surface wettability. In particular, the hydrophobic surface ($\theta_e = 120°$) exhibited a higher density of small drops (r < 20 μm) and a smaller departing

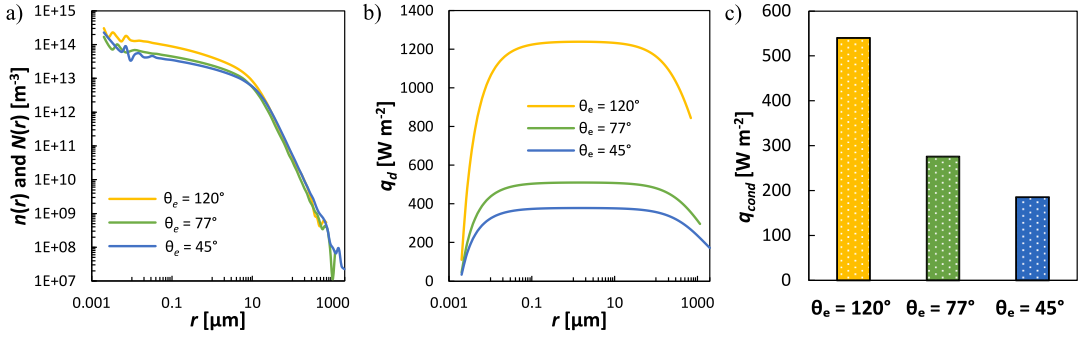

Fig. 11. Results of the simulations performed by the present model coupled with Zheng et al. [17] for the study of wettability effect. a) Calculated drop-size distribution, b) heat flux through an individual drop and c) average q_{cond} for different equilibrium contact angle (θ_e = 45°, 77°, 120°). The contact angle hysteresis is fixed at 20°, N_s at 7 × 10^8 m^{-2} and α at 10^{-4}. The other inputs are listed in Table 3.

radius compared to the baseline hydrophilic surface ($\theta_e = 77°$). However, the resulting increase in average latent heat flux, from 270 W m^{-2} to 540 W m^{-2} (+100%), was mainly due to a change in the heat flux transferred by the individual drops. These results contribute to fill the gap in the literature regarding the population of small drops during DWC from humid air.

CRediT authorship contribution statement

Matteo Mirafiori: Writing – original draft, Software, Methodology, Investigation, Formal analysis. **Marco Tancon:** Writing – review & editing, Writing – original draft, Visualization, Validation, Methodology, Investigation, Formal analysis. **Stefano Bortolin:** Writing – review & editing, Supervision, Resources, Funding acquisition, Conceptualization. **Davide Del Col:** Writing – review & editing, Supervision, Methodology, Funding acquisition, Conceptualization.

Declaration of competing interest

The authors declare the following financial interests/personal relationships which may be considered as potential competing interests:

Stefano Bortolin reports financial support was provided by European Union - Next Generation EU and Italian Ministry for University and Research (MUR) through the project PRIN 2022 (2022PSPA8R) WADERE. If there are other authors, they declare that they have no known competing financial interests or personal relationships that could have appeared to influence the work reported in this paper.

Data availability

Data will be made available on request.

Acknowledgements

The Department of Industrial Engineering of the University of Padova is acknowledged for the financial support through the BIRD 228237 (2022). Financial support of European Union - Next Generation EU and Italian Ministry for University and Research (MUR) through the project PRIN 2022 (2022PSPA8R) WADERE is gratefully acknowledged.

Appendix A. Supplementary data

Supplementary data to this article can be found online at https://doi.org/10.1016/j.icheatmasstransfer.2024.107905.

References

[1] M. Fujiwara, K. Takahashi, K. Takagi, Improvement of condensation step of water vapor in solar desalination of seawater and the development of three-ply membrane system, Desalination 508 (2021) 115051, https://doi.org/10.1016/j.desal.2021.115051.
[2] K. Egab, M. Alwazzan, B. Peng, S.K. Oudah, Z. Guo, X. Dai, J. Khan, C. Li, Enhancing filmwise and dropwise condensation using a hybrid wettability contrast mechanism: circular patterns, Int. J. Heat Mass Transf. 154 (2020) 119640, https://doi.org/10.1016/j.ijheatmasstransfer.2020.119640.
[3] R. Parin, M. Tancon, M. Mirafiori, S. Bortolin, L. Moro, L. Zago, F. Carraro, A. Martucci, D. Del Col, Heat transfer and droplet population during dropwise condensation on high durability coatings, Appl. Therm. Eng. 179 (2020) 115718, https://doi.org/10.1016/j.applthermaleng.2020.115718.
[4] F. Lv, S. Lin, H. Nie, Z. Dong, F. Zhao, D. Cheng, Z. Dong, R. Gulfam, Droplet dynamics and heat transfer enhancement via dropwise condensation on helically-finned hydrophobic tube, Int. Commun. Heat Mass Transf. 135 (2022) 106153, https://doi.org/10.1016/J.ICHEATMASSTRANSFER.2022.106153.
[5] J.W. Rose, Dropwise condensation theory and experiment: a review, Proc. Inst. Mech. Eng. Part A J. Power Energy. 216 (2002) 115–128, https://doi.org/10.1243/09576500260049034.
[6] M. Basso, E. Colusso, M. Tancon, S. Bortolin, M. Mirafiori, M. Guglielmi, D. Del Col, A. Martucci, Hydrophobic hybrid silica sol-gel coating on aluminium: stability evaluation during saturated vapour condensation, J. Non-Crystalline Solids X. 17 (2023) 100143, https://doi.org/10.1016/J.NOCX.2022.100143.
[7] E. Colusso, M. Tancon, L. Cazzola, R. Parin, S. Agnoli, F. De Boni, M.G. Pelizzo, E. Della Gaspera, D. Del Col, A. Martucci, Solution-processed graphene oxide coatings for enhanced heat transfer during dropwise condensation of steam, Nano Sel. 2 (2021) 61–71, https://doi.org/10.1002/nano.202000105.
[8] M. Tancon, M. Mirafiori, S. Bortolin, R. Parin, E. Colusso, A. Martucci, D. Del Col, Simultaneous measurement of heat flux and droplet population during dropwise condensation from humid air flowing on a vertical surface, Exp. Thermal Fluid Sci. 136 (2022) 110677, https://doi.org/10.1016/j.expthermflusci.2022.110677.
[9] K.S. Yang, K.H. Lin, C.W. Tu, Y.Z. He, C.C. Wang, Experimental investigation of moist air condensation on hydrophilic, hydrophobic, superhydrophilic, and hybrid hydrophobic-hydrophilic surfaces, Int. J. Heat Mass Transf. 115 (2017) 1032–1041, https://doi.org/10.1016/j.ijheatmasstransfer.2017.08.112.
[10] S. Wang, X. Yu, C. Liang, Y. Zhang, Enhanced condensation heat transfer in air-conditioner heat exchanger using superhydrophobic foils, Appl. Therm. Eng. 137 (2018) 758–766, https://doi.org/10.1016/J.APPLTHERMALENG.2018.04.020.
[11] S. Kim, K.J. Kim, Dropwise condensation modeling suitable for superhydrophobic surfaces, J. Heat Transfer 133 (2011) 1–8, https://doi.org/10.1115/1.4003742.
[12] N. Miljkovic, R. Enright, E.N. Wang, Modeling and optimization of Superhydrophobic condensation, J. Heat Transfer 135 (2013) 111004, https://doi.org/10.1115/1.4024597.
[13] S.F. Zheng, Z.Y. Wu, G.Q. Liu, Y.R. Yang, B. Sundén, X.D. Wang, The condensation characteristics of individual droplets during dropwise condensation, Int. Commun. Heat Mass Transf. 131 (2022) 105836, https://doi.org/10.1016/J.ICHEATMASSTRANSFER.2021.105836.
[14] E.J. Le Fevre, J.W. Rose, A theory of heat transfer by dropwise condensation, in: Proc. 3rd Int. Heat Transf. Conf Vol. 2, 2019, pp. 362–375, https://doi.org/10.1615/ihtc3.180.
[15] H. Tanaka, A theoretical study of dropwise condensation, J. Heat Transfer 97 (1975) 72–78, https://doi.org/10.1115/1.3450291.
[16] M. Tancon, A. Abbatecola, M. Mirafiori, S. Bortolin, E. Colusso, A. Martucci, D. Del Col, Investigation of surface inclination effect during dropwise condensation of flowing saturated steam, Int. J. Therm. Sci. 196 (2024) 108738, https://doi.org/10.1016/J.IJTHERMALSCI.2023.108738.
[17] S. Zheng, F. Eimann, C. Philipp, T. Fieback, U. Gross, Modeling of heat and mass transfer for dropwise condensation of moist air and the experimental validation, Int. J. Heat Mass Transf. 120 (2018) 879–894, https://doi.org/10.1016/j.ijheatmasstransfer.2017.12.059.
[18] V. Baghel, B.S. Sikarwar, K. Muralidhar, Dropwise condensation from moist air over a hydrophobic metallic substrate, Appl. Therm. Eng. 181 (2020), https://doi.org/10.1016/j.applthermaleng.2020.115733.
[19] N. Lyu, H. He, J. Zhang, F. Wang, C. Liang, X. Zhang, Investigation on the growth characteristics of condensed droplet clusters on superhydrophobic surface within humid air, Energ. Buildings 261 (2022) 111978, https://doi.org/10.1016/j.enbuild.2022.111978.
[20] M. Mei, F. Hu, C. Han, Ergodic simulation of droplet growth during dropwise condensation, Appl. Therm. Eng. 236 (2024) 121929, https://doi.org/10.1016/J.APPLTHERMALENG.2023.121929.
[21] G. Croce, N. Suzzi, Numerical simulation of dropwise condensation of steam over hybrid surfaces via new non-dimensional heat transfer model, Fluids 8 (2023) 300, 8 (2023) 300, https://doi.org/10.3390/FLUIDS8110300.
[22] M. Mirafiori, M. Tancon, S. Bortolin, D. Del Col, Modeling of growth and dynamics of droplets during dropwise condensation of steam, Int. J. Heat Mass Transf. 222 (2024) 125109, https://doi.org/10.1016/j.ijheatmasstransfer.2023.125109.
[23] K.A. Stevens, J. Crockett, D. Maynes, B.D. Iverson, Simulation of drop-size distribution during dropwise and jumping drop condensation on a vertical surface: implications for heat transfer modeling, Langmuir 35 (2019) 12858–12875, https://doi.org/10.1021/acs.langmuir.9b02232.
[24] J. Lethuillier, P. Lavieille, M. Miscevic, About the role of falling droplets' sweeping in surface renewal during dropwise condensation, Langmuir 36 (2020) 12877–12886, https://doi.org/10.1021/acs.langmuir.0c02092.
[25] S. Zheng, F. Eimann, C. Philipp, T. Fieback, U. Gross, Experimental and modeling investigations of dropwise condensation out of convective humid air flow, Int. J. Heat Mass Transf. 151 (2020) 119349, https://doi.org/10.1016/j.ijheatmasstransfer.2020.119349.
[26] R. Marek, J. Straub, Analysis of the evaporation coefficient and the condensation coefficient of water, Int. J. Heat Mass Transf. 44 (2001) 39–53, https://doi.org/10.1016/S0017-9310(00)00086-7.
[27] K. Gleason, H. Voota, S.A. Putnam, Steady-state droplet evaporation: contact angle influence on the evaporation efficiency, Int. J. Heat Mass Transf. 101 (2016) 418–426, https://doi.org/10.1016/J.IJHEATMASSTRANSFER.2016.04.075.
[28] J.E. Castillo, J.A. Weibel, S.V. Garimella, The effect of relative humidity on dropwise condensation dynamics, Int. J. Heat Mass Transf. 80 (2015) 759–766, https://doi.org/10.1016/J.IJHEATMASSTRANSFER.2014.09.080.
[29] R.N. Leach, F. Stevens, S.C. Langford, J.T. Dickinson, Dropwise condensation: experiments and simulations of nucleation and growth of water drops in a cooling system, Langmuir 22 (2006) 8864–8872, https://doi.org/10.1021/la061901+.
[30] S. Zheng, F. Eimann, C. Philipp, T. Fieback, U. Gross, Dropwise condensation in the presence of non-condensable gas: interaction effects of the droplet array using the distributed point sink method, Int. J. Heat Mass Transf. 141 (2019) 34–47, https://doi.org/10.1016/j.ijheatmasstransfer.2019.06.068.
[31] J.E. Castillo, J.A. Weibel, A point sink superposition method for predicting droplet interaction effects during vapor-diffusion-driven dropwise condensation in humid air, Int. J. Heat Mass Transf. 118 (2018) 708–719, https://doi.org/10.1016/j.ijheatmasstransfer.2017.11.045.
[32] N. Suzzi, G. Croce, Numerical simulation of dropwise condensation over hydrophobic surfaces using vapor-diffusion model, Appl. Therm. Eng. 214 (2022) 118806, https://doi.org/10.1016/J.APPLTHERMALENG.2022.118806.

[33] G.T. Barnes, Insoluble monolayers and the evaporation coefficient of water-reply to comments, J. Colloid Interface Sci. 65 (1978) 576–577, https://doi.org/10.1016/0021-9797(78)90112-1.
[34] E.E. Gose, A.N. Mucciardi, E. Baer, Model for dropwise condensation on randomly distributed sites, Int. J. Heat Mass Transf. 10 (1967) 15–22, https://doi.org/10.1016/0017-9310(67)90180-9.
[35] L.R. Glicksman, A.W. Hunt, Numerical simulation of dropwise condensation, Int. J. Heat Mass Transf. 15 (1972) 2251–2269, https://doi.org/10.1016/0017-9310(72)90046-4.
[36] S. Bortolin, M. Tancon, D. Del Col, Heat transfer enhancement during dropwise condensation over wettability-controlled surfaces, Surf. Wettability Eff. Phase Chang. (2022) 29–67, https://doi.org/10.1007/978-3-030-82992-6_3.
[37] G. Chkonia, J. Wölk, R. Strey, J. Wedekind, D. Reguera, Evaluating nucleation rates in direct simulations, J. Chem. Phys. 130 (2009), https://doi.org/10.1063/1.3072794/565065.
[38] D.T.S. Ranathunga, A. Shamir, X. Dai, S.O. Nielsen, Molecular dynamics simulations of water condensation on surfaces with tunable wettability, Langmuir 36 (2020) 7383–7391, https://doi.org/10.1021/ACS.LANGMUIR.0C00915/ASSET/IMAGES/LARGE/LA0C00915_0006.JPEG.
[39] K. Yasuoka, M. Matsumoto, Molecular dynamics of homogeneous nucleation in the vapor phase. II. Water, J. Chem. Phys. 109 (1998) 8463–8470, https://doi.org/10.1063/1.477510.
[40] D. Niu, H. Gao, G. Tang, Y. Yan, Droplet nucleation and growth in the presence of noncondensable gas: a molecular dynamics study, Langmuir 37 (2021) 9009–9016, https://doi.org/10.1021/acs.langmuir.1c00961.
[41] T. Andrews, Computation time comparison between Matlab and C++ using launch windows, Aerosp. Eng. (2012) 1–6. https://digitalcommons.calpoly.edu/aerosp/78 (accessed July 21, 2022).
[42] E.W. Lemmon, M.L. Bell, I.H. Huber, M.O. McLinden, NIST Standard Reference Database 23: Reference Fluid Thermodynamic and Transport Properties-REFPROP, Version 10.0, 2018, https://doi.org/10.18434/T4/1502528.
[43] A. Katselas, R. Parin, C. Neto, Quantification of nucleation site density as a function of surface wettability on smooth surfaces, Adv. Mater. Interfaces (2022) 2200246, https://doi.org/10.1002/ADMI.202200246.
[44] M. Tancon, R. Parin, S. Bortolin, A. Martucci, D. Del Col, Effect of steam velocity during dropwise condensation, Int. J. Heat Mass Transf. 165 (2021) 120624, https://doi.org/10.1016/j.ijheatmasstransfer.2020.120624.
[45] M. Tancon, M. Mirafiori, S. Bortolin, M. Basso, E. Colusso, D. Del Col, Dropwise condensation mechanisms when varying vapor velocity, Appl. Therm. Eng. 216 (2022) 119021, https://doi.org/10.1016/J.APPLTHERMALENG.2022.119021.
[46] J. Xie, J. Xu, W. Shang, K. Zhang, Mode selection between sliding and rolling for droplet on inclined surface: effect of surface wettability, Int. J. Heat Mass Transf. 122 (2018) 45–58, https://doi.org/10.1016/j.ijheatmasstransfer.2018.01.098.
[47] R. Parin, M. Rigon, S. Bortolin, A. Martucci, D. Del Col, Optimization of hybrid sol-gel coating for dropwise condensation of pure steam, Mater 13 (2020) 878, 13 (2020) 878, https://doi.org/10.3390/MA13040878.
[48] M. Basso, E. Colusso, A. Sacco, M. Tancon, S. Bortolin, M. Mirafiori, M. Guglielmi, A. Martucci, Bioinspired silica-based sol–gel micropatterns on aluminium for humid air condensation, J. Sol-Gel Sci. Technol. 102 (2022) 466–477, https://doi.org/10.1007/S10971-022-05771-7/FIGURES/6.
[49] Joint Committee for Guides in Metrology, Evaluation of Measurement Data - Guide to the Expression of Uncertainty in Measurement. www.bipm.org, 2008 (accessed April 15, 2020).